

PAPER View Article Online



Cite this: DOI: 10.1039/c9an01186b

Effects of surface treatments on trapping with DC insulator-based dielectrophoresis†

Claire V. Crowther, **D **a Viola Sanderlin, **D Mark A. Hayes **D a and Gillian H. Gile **D b

A central challenge in measuring the biophysical properties of cells with electrokinetic approaches is the assignment of these biophysical properties to specific biological characteristics. Changes in the electrokinetic behavior of cells may come from mutations, altered gene expression levels, post-translation modifications, or environmental effects. Here we assess the electrokinetic behavior of chemically surface-modified bacterial cells in order to gain insight into the biophysical properties that are specifically affected by changes in surface chemistry. Using *E. coli* as a scaffold, an amine coupling reaction was used to covalently attach glycine, spermine, bovine serum albumin (protein), or 7-amino-4-methyl-3-coumarinyl-acetic acid (fluorescent dye) to the free carboxylic acid groups on the surface of the cells. These populations, along with unlabeled control cells, were subject to electrokinetic and dielectrophoretic measurements to quantify any changes in the biophysical properties upon alteration. The properties associated with each electrokinetic force are discussed relative to the specific reactant used. We conclude that relatively modest and superficial changes to cell surfaces can cause measurable changes in their biophysical properties.

Received 27th June 2019, Accepted 25th October 2019 DOI: 10.1039/c9an01186b

rsc.li/analyst

Introduction

Complex biological mixtures of interest abound. Separating these mixtures into component parts finds applications in agriculture and food safety, pharmaceutical and vaccine development, forensics, blood-based diagnostics, viral isolation, and environmental samples. Many different separations science techniques have been developed for the isolation of analytes of interest, each with its own advantages and disadvantages. At the forefront of these is the ability to precisely and accurately sort cells based on their biophysical properties.^{1–11}

Dielectrophoresis (DEP) is a force that acts on a polarizable particle in a non-uniform electric field. Because it does not require high voltages, DEP can be used to manipulate living cells while preserving their viability. The effects of DEP are highly sensitive to the intrinsic biophysical properties of cells (Fig. 1). The ability to isolate a cell type of interest with high specificity, even if it is present in low concentrations, is a major advantage of DEP separations. 19,22,23

Many DEP systems utilize embedded electrodes, known as eDEP, to manipulate analytes of interest. 4,15,24,25 However,

eDEP is subject to electrode fouling, undesirable electrolysis, and the DEP force is only effective very close to the electrodes where the electric field gradients are high. In the early 2000s insulator-based dielectrophoresis (iDEP) was introduced, which uses insulating features to manipulate the electric field between distal electrodes. ^{18,26,27} Electrode placement in the distal reservoirs limits the effects of fouling and electrolysis. iDEP has been successful in manipulating, differentiating, and isolating various cells, including various strains of *E. coli*, ²⁸ antibiotic resistant and sensitive *Staphylococcus epidermidis*, ² *Bacillus subtilis*, ²⁹ and *Pseudomonas aeruginosa* and *Streptococcus mitis*. ³⁰

The interaction of a cell with its environment is determined by its surface properties (Fig. 1). Specifically, the physiochemical properties are shaped by surface biomolecules that are in turn shaped by gene expression. For example, the pathogenic bacterium *Salmonella* regulates and modifies its membrane composition as needed for protection or host invasion. Similarly, the physiochemical properties of the yeast cell wall determine its propensity for adhesion and flocculation. Importantly, changes in cell surface functional groups influence dielectrophoretic mobility. The ability of iDEP to detect changes in the both the internal and surface properties of a cell have resulted in its growth as a field for interrogating and separating cells. 17,34

The biophysical properties of *E. coli* define its behavior in a DEP system. Within the system two main forces are considered, electrokinesis and dielectrophoresis. The electroki-

^aSchool of Molecular Sciences, Arizona State University, Tempe, Arizona, USA. E-mail: cvcrowth@asu.edu: Tel: +1 (303)-941-2891

^bSchool of Life Sciences, Arizona State University, Tempe, Arizona, USA

[†]Electronic supplementary information (ESI) available. See DOI: 10.1039/c9an01186b

Periplasm Cytoplasm Fimbriae Flagella Cell Peptido-Outer Membrane Membrane glycan Membrane protein Lipopoly-Lipoprotein saccharides

Fig. 1 Illustration of physical structure of *E. coli*, a Gram-negative bacterium, focusing on outer layers. Surface modifications can affect the biophysical properties of the cell and thus the electrokinetic and dielectrophoretic mobilities.

netic (EK) force is dominated by the zeta potential of the surface of the cell defined by the cell surface charge density and buffer properties. For a direct current (DC) electric field, the DEP force is described by the conductivity of the cell and its immediate environment (electric double layer) compared to bulk buffer conductivity. E. coli is gram-negative and its cell wall includes an outer membrane (7-8 nm) and a thin peptidoglycan layer (1-3 nm) (Fig. 1).35,36 This is in contrast with gram-positive bacteria, which have a peptidoglycan layer ranging from 20-80 nm in thickness and no outer membrane. 35,36 When E. coli is subjected to a DC electric field, the conductivities of the different layers define the forces that the cell experiences. The conductivities of the cell wall and cell membrane have been reported as 5×10^2 and 5×10^{-5} µS mm⁻¹, respectively.³⁷ As the cell wall is highly conductive, an electric field can easily penetrate it.

Several studies on *E. coli* strains have measured EP or EK and DEP. In terms of EP, *E. coli* has a high density of negative charges on its surface resulting in a net negative charge at physiological pH, and a higher electrophoretic mobility than Gram-positive bacteria. Also, the EK mobilities of *E. coli* strains do not differ significantly, but the zeta potential fluctuates, depending on pH, between -40 to -80 mV. An iDEP study of live *versus* dead *E. coli* concluded that size, shape, and other morphological characteristics do not differ between the live and dead bacteria, however the conductivity of the cell membranes differed, which altered the DEP force the cells experienced. There are minimal variations in EP mobility with iDEP experiments, but serotypes can be differentiated in balance with EK.

The current work addresses the effect of chemical surface modifications of viable *E. coli* cells on the cellular biophysical properties as measured by iDEP. The quantification is reduced to fundamental values for electrokinetic and dielectrophoretic mobilities which can be correlated and interpreted in terms of the known changes in cell surface chemistry. Differences were observed for both mobilities according to the surface alterations, which is consistent with changes in the zeta potential

(EK) and/or conductivity of the cell system (DEP). These results demonstrate that the iDEP system provides for a sensitive and quantitative measurement of known and specific chemical alterations of *E. coli*.

Theory

Insulator-based dielectrophoresis manipulates analytes based on the intrinsic properties of the analyte and the effects induced in the microchannel by the electrokinetic and dielectrophoretic forces. In-depth development of the particle properties and forces are presented in several previous works.^{7,20,42-45}

The electrokinetic properties of a given analyte can be described by the electrokinetic mobility (μ_{EK}) which combines the effects of electrophoretic mobility (μ_{EP}) and electroosmosis (μ_{EO}).

$$\mu_{\rm EK} = (\mu_{\rm EO} + \mu_{\rm EP}) = \frac{-\varepsilon_{\rm m}\zeta_{\rm m}}{\eta} + \frac{\varepsilon_{\rm m}\zeta_{\rm p}}{\eta} = \frac{-\varepsilon_{\rm m}(\zeta_{\rm m} - \zeta_{\rm p})}{\eta} \tag{1}$$

where $\varepsilon_{\rm m}$ is the permittivity of the medium, $\zeta_{\rm m}$ and $\zeta_{\rm p}$ are the zeta potential of the medium and particle, respectively, and η is the viscosity of the medium. The electrokinetic velocity of a given analyte can therefore be described by the following:

$$\vec{\nu}_{\rm EK} = \mu_{\rm EK} \vec{E} \tag{2}$$

Similarly, the dielectrophoretic mobility (μ_{DEP}) of an analyte can be described by the following:

$$\mu_{\rm DEP} = \frac{\varepsilon_{\rm m} r^2 f_{\rm CM}}{3\eta} \tag{3}$$

where r is the radius of the particle and $f_{\rm CM}$ is the Clausius–Mossotti factor, which is based on the conductivity of the particle and medium in DC fields.

The movement, flux (j), of a given analyte in a the microchannel can be described using a combination of the effects of

Analyst Paper

diffusion (D), concentration (C), and the bulk $(\bar{\nu}_{\text{Bulk}})$, electrokinetic (\vec{v}_{EK}) , and dielectrophoretic (\vec{v}_{DEP}) velocities. The \vec{v}_{EK} and $\vec{\nu}_{DEP}$ relate their corresponding mobilities with the electric field (\vec{E}) or the gradient of the electric field squared $(\nabla |\vec{E}|^2)$, respectively. The effects of D can be disregarded as E. coli is larger than 1 μ m, and $\vec{\nu}_{Bulk}$ can be ignored as pressure driven flow is experimentally eliminated. Therefore, the movement of a given analytes in a microchannel can be described by the following.

$$\vec{j} = D\nabla C + C(\vec{\nu}_{\text{Bulk}} + \vec{\nu}_{\text{EK}} + \vec{\nu}_{\text{DEP}}) \approx C(\vec{\nu}_{\text{EK}} + \vec{\nu}_{\text{DEP}})$$
 (4)

The DEP force (\vec{F}_{DEP}) describes the force on a polarizable particle in a non-uniform electric field. As E. coli is rod shaped, the dielectrophoretic force for ellipsoidal particles is considered to account for the effect of the dimensions.46,47

$$\vec{F}_{\text{DEP}} = \frac{4}{3} \pi abc \varepsilon_{\text{m}} \left(\frac{\sigma_{\text{p}} - \sigma_{\text{m}}}{Z \sigma_{\text{p}} + (1 - Z) \sigma_{\text{m}}} \right) \nabla \left| \vec{E} \right|^{2}$$
 (5)

where the semi-principal axes of the ellipsoid are represented by a, b and c (a > b = c), Z is the depolarization factor, σ is the conductivity of the particle (p) or media (m). The direction of the F_{DEP} , depends on the conductivities of both the particle and media to determine whether the analyte of interest experiences positive or negative dielectrophoresis. When a DC potential is applied, if the conductivity of the particle is greater than the conductivity of the media, the particle will be attracted to areas of high electric field strength, resulting in positive dielectrophoresis. Whereas, when the conductivity of the media is greater than that of particle, the particle is repelled from high electric field strengths, resulting in negative dielectrophoresis. The experimental setup in this study results in negative dielectrophoretic trapping.

As E. coli is made up of several layers, including the cytoplasm, plasma membrane, and cell wall, a multi-shell model is employed to better account for the variations in conductivities between layers. 48-51

DEP trapping of analytes occurs when the flux of the particle along the electric field lines is zero, $j \cdot E = 0$, which can be described using the EK and DEP mobilities base on eqn (4).

$$\frac{\left|\nabla\left|\vec{E}\right|^{2}}{E^{2}} \cdot \vec{E} \ge \frac{\mu_{\text{EK}}}{\mu_{\text{DEP}}} \tag{6}$$

The behavior of a given analyte in the microchannel can be used to assess its biophysical properties by understanding the EK and DEP mobilities.

Modeling

Finite element multiphysics

Finite element modeling (COMSOL, Inc., Burlington, MA) of the distribution of the electric field in the microchannel was performed as previously detailed.42 The AC/DC module was

used to interrogate the \vec{E} , $\nabla \left| \vec{E} \right|^2$, and $\frac{\nabla \left| \vec{E} \right|^2}{F^2} \cdot \vec{E}$ in an accurately scaled 2D model of the microchannel. The accuracy of the computations may be affected as the surface charge between PDMS and silica likely differ.

Data model

To quantify the behavior of a given analyte in the system, we employ a model that uses signal intensity (I_s) to assess both the time required for particle trapping at a constant voltage and the voltage required for trapping at a fixed time point for a given gate of interest. The data model for the microchannel utilized in this paper has previously been developed and applied.17,52 Briefly, the time-dependent model, where the applied potential is held constant can be represented by:

$$I_{\rm s} = \frac{24V_{\rm A}\gamma n\mu_{\rm Ek}wh}{\rm s}t\tag{7}$$

where V_A is the applied potential, γ is the average I_S per particle, n is the concentration of the analyte of interest, w is the average width of the microchannel an analyte experiences, h is the height of the microchannel, s is a stacking factor, and t is the time for which the potential has been applied. Both w and s are treated as adjustable parameters. Channel design and velocity of the analyte will affect the w which an analyte experiences. For the channel used in this paper the gradient nature will alter the w experienced by an analyte. While s is dependent on the number of stacked particles at a given gate, which is dependent on the size and interactions of the bacteria.

The time dependent model can be manipulated by holding the time a given potential has been applied constant and varying the voltage, resulting in a voltage-dependent model. This is described using a piecewise function:

$$\begin{split} I_{\rm S}(V_{\rm A}) &= \\ & \left\{ \begin{array}{c} 0, \ {\rm if} \ V_{\rm A} < \frac{1}{1.0 \times 10^7} \left(\frac{\mu_{\rm EK}}{\mu_{\rm DEP}}\right) \\ 24 \frac{\gamma n \mu_{\rm Ek} w h t}{s} \left[V_{\rm A} - \frac{1}{1.0 \times 10^7} \left(\frac{\mu_{\rm EK}}{\mu_{\rm DEP}}\right) \right], \ {\rm if} \ V_{\rm A} \geq \frac{1}{1.0 \times 10^7} \left(\frac{\mu_{\rm EK}}{\mu_{\rm DEP}}\right) \\ \end{array} \right. \end{split}$$

where at potentials when no trapping occurs, there is no contribution to the $I_s(V_A)$, but after a given onset potential (c), the analyte will collect in a linear fashion, because the transport of the analyte to its trapping location will be dominated by $\bar{\nu}_{\rm EK}$ (eqn (2)).

Materials and methods

Device fabrication

Soft photolithography and microchannel formation via oxygen plasma bonding were performed according to established procedures. The V1 sawtooth microchannel geometry has been described in prior publications.^{28,53-55} It consists of a 4.2 cm long microchannel, with an average depth of 17 µm, where Paper

Fig. 2 Amide coupling reaction (A) for *E. coli* surface modifications and molecular structures (B) coupled to the *E. coli* (C). ⁵⁸ *E. coli* exhibits negative dielectrophoretic trapping at the first 27 µm gate in the microchannel (C). Data shown is from glycine-modified *E. coli* after approximately 8 seconds with an applied potential of –500 V. The green box represents the ROI which was analyzed for signal intensity.

equilateral triangles line both walls, forming opposing teeth that create constriction points, referred to hereafter as gates. The triangles increase in size from the inlet to the outlet, producing gates that gradually decrease in size, focusing toward the centerline. Each gate size is repeated six times before decreasing in size. The initial gate width is 945 μm , with the sides of the equilateral triangles increasing by 40 μm after every six gates, resulting in a final gate width of 27 μm (Fig. 2C).

Polydimethylsiloxane (PDMS) microchannels were cast using Sylgard 184 silicone elastomer kit (Dow Silicones Corporation, Midland, MI USA) and cured at 70 °C for 1 h. After curing, 3 mm reservoir holes were punched to form the inlet and outlet reservoirs. Microchannels were stored in airtight plastic bags in the freezer for up to two weeks prior to use. For experimentation, PDMS casts were washed with isopropanol then 18 M Ω water followed by a 30 s sonication in 18 M Ω water, and then dried with air. Glass slides were cleaned in the same manner, except that an acetone wash preceded the isopropanol wash. Bonding of a completed microdevice was done by treating both the glass slides and the PDMS casts with oxygen plasma (PDC-32G, Harrick Plasma, Ithaca, NY) for 60 seconds at 18 W.

Cell culture and surface modification

Escherichia coli strain Bl21 DE3 Star with plasmid pET-29 expressing superfolder GFP (sfGFP) was grown on Lysogeny broth (LB) agar plates with 50 μg mL $^{-1}$ kanamycin to maintain the plasmid. For each treatment, a single colony was inoculated into 10 mL of LB broth with 50 μg mL $^{-1}$ kanamycin incubated overnight in shaker at 37° C to late log phase. Once the culture reached an OD₆₀₀ between 0.8–1.1 the culture was

inoculated with 1 mM isopropyl-*b*-D-1-thiogalactopyranosid (IPTG). This induces the lac promoter expression of sfGFP and reduces cell growth as the protein expression is metabolically taxing on the bacteria. The cells were then incubated for 2 more hours. The bacteria were then stored at 4 °C for at least an hour prior to labeling, to minimize cell growth.

Siegmund and Wöstemeyer developed a surface modification technique for bacteria which was modified for this work. ^{56,57} A carbodiimide (*N*-(3-dimethylaminopropyl)-*N*-ethylcarbodiimide hydrochloride (EDC)) is used to covalently link compounds to the cell's surface (Fig. 2A). The following molecules were used for surface modification: glycine, bovine serum albumin (BSA), spermine, and 7-amino-4-methyl-3-coumarinylacetic acid (AMCA-H) (Fig. 2B). AMCA-H was used to visualize a successful surface labeling reaction, where a color change of the *E. coli* was observed resulting from the fluorescent AMCA-H being bound to the *E. coli*'s surface. ^{56,57}

For surface modifications, a solution of EDC (10 mg mL $^{-1}$) was made fresh with 18 M Ω water. A volume of 1 mL of the overnight culture was washed three times with 1 mL saline (9 g L $^{-1}$ NaCl, 0.2 µm filtered) and resuspended in saline. EDC was added to the washed cells for a final concentration of 1 mg mL $^{-1}$ with a total volume of 1 mL and then incubated on a shaker for 10 minutes at room temperature. The desired molecule for modification was then added for a final concentration of 1 mM, except in the case of BSA when a final concentration of 10 mg mL $^{-1}$ was used. The pH was tested and adjusted using ~0.1 M phosphoric acid to pH ~5 to reach a pH between 4 and 6 to achieve optimal coupling. Adjustments in pH were only necessary for spermine modified cells. The reaction was then incubated for 20 additional minutes at room temperature. The modified cells were then washed three times and

resuspended in saline, with 1 mM glycine added to block any excess EDC binding, and incubated at room temperature for 10 minutes. The cells were washed three times in saline and resuspended with 2 mM phosphate buffer (PB); where the PB had a measured conductivity of 330 μS cm⁻¹. The modified cells were stored at 4 °C overnight. For experimentation, the next day, the modified cells were vortexed and a dilution of 200 µL of the modified cells into 800 µL of 2 mM PB was made.

The viability of the E. coli after surface modification was determined for two separate colonies picked from the LB-agar/ kanamycin plates. For each surface modification of each colony a liquid culture was made from 10 µL of the washed, surface modified cells in phosphate buffer and 50 µg mL⁻¹ kanamycin which was incubated overnight in shaker at 37° C to late log phase and inoculated with IPTG as described previously. The surface modified E. coli culture was also streaked on an LB agar plate with 50 μg mL⁻¹ kanamycin. The plate was incubated at room temperature and was checked every 24 hours for three days for colony growth and sfGFP expression (ESI†).

Microfluidic experimental manipulation

Microdevices were washed and bonded on the day of use. For each trial a new microdevice was utilized. Multiple replicate trials $(n \ge 9)$ were run for each surface modification and for unmodified control cells. The inlet and outlet reservoirs of the microchannel were filled with 15 µL of 2 mM PB and allowed to stand for 10 minutes. Platinum electrodes (0.404 mm external diameter 99.9% purity, Alfa Aesar, Ward Hill, MA, USA) were placed in both reservoirs and attached to a power supply (HVS 448 High Voltage Sequencers, LabSmith Inc., Livermore, CA, USA). The 2 mM PB was then removed and 15 μ L of the modified diluted cell suspension was placed in the inlet reservoir, allowing the cell suspension to fill the channel by pressure driven flow for 5 minutes. The outlet reservoir was then filled with 15 µL of 2 mM PB to balance pressure driven flow. Fluorescence microscopy (Olympus IX70) with a mercury short arc lamp (H30 102 w/2, OSRAM) and an Olympus DAPI, FITC, Texas Red triple band pass cube (Olympus, Center Valley, PA, USA) was used to check the presence of bacteria in the microchannel as the E. coli's expression of sfGFP results in excitation/emission properties of 485/510 nm. 59 Experiments with the microchannel were monitored using bright field microscopy with a 4× objective. Voltages were sequentially applied from -100 to -900 V for ~30 s to characterize how surface modifications affected the cell's behavior. Images were captured using Streampix V image capture software (Norpix, Inc., Montreal, QC) via a QICAM cooled CCD camera (QImaging, Inc., Surrey, BC). Trials were run for each surface modification as a singular analyte, where the magnitude (V_A) and duration (t_A) of applied potential was varied.

Image analysis

To assess the trapping behavior of the bacteria in the microchannel, I_s (arbitrary units) for a defined region of interest (ROI) was monitored at the 27 µm gate both in response to the magnitude of the potential and the length of time a potential was applied to the system. The ROI was defined as an 80×50 pixel box near the 27 µm gate where trapping characteristically is observed (Fig. 2C, green box). The $I_{\rm s}$ determinations were performed using ImageJ (NIH freeware) and normalized for E. coli concentration within each run and signal present prior to the application of voltage. A measurement 2 s after commencing data recording for the -100 V trial was used to for the measurement of the background I_s with no applied voltage, as the voltage was not applied to system until ~5 s into recording.

The velocity of the modified cells was measured using particle tracing, where the path of an individual bacterium was traced from frame-to-frame at or near the centerline just prior to the 27 μ m gate (n = 3 for each surface modification). Each particle was traced until it could no longer be identified in the subsequent frame or reached a point where DEP could influence its velocity.

When utilizing the time-dependent data model the I_s at a given time point is used rather than an average. This can lead to instances where statistically significant trapping is occurring (Fig. 3, red data points), but for a given trial a negative I_s is recorded. These were excluded for interpretation as trapping was not occurring in for the specific individual trial. This may be due to several different reasons: (1) a given trial had to yet experienced its onset potential which can be a result of several different factors (residual pressure driven flow artificially increasing the EK force, variations in the buffer solution, etc.) and (2) an aggregate clearing the trapped material prior to assessment. Therefore, when assessing μ_{EK} with the timedependent model, data points where the I_s was determined to be negative for a unique trial were excluded.

Safety considerations

The bacterial strain used in this study is classified as Bio Safety Level 1 (BSL1). Experiments were conducted in accordance with the current version of the CDC/NIH BMBL publication in an approved BSL 1 laboratory.

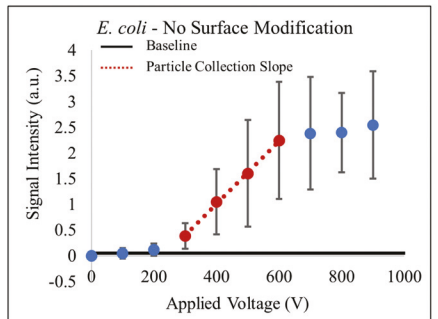
Results

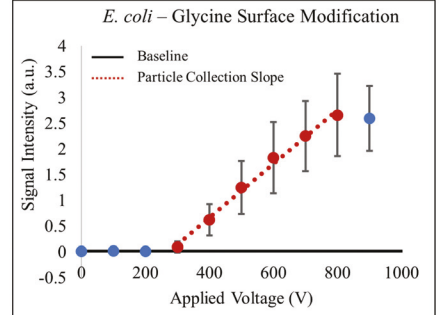
The biophysical behavior of E. coli with four different surface modifications was quantified using iDEP. Four distinct compounds, glycine, spermine, BSA, and AMCA-H, were covalently linked to the carboxyl groups on the surface of the E. coli using an amine coupling reaction. The surface modified E. coli were determined to be viable except for those modified with AMCA-H (ESI†).

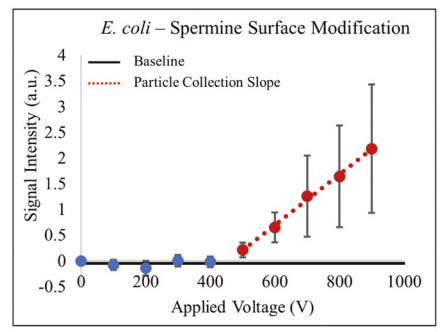
Velocity and electrokinetic mobility determination

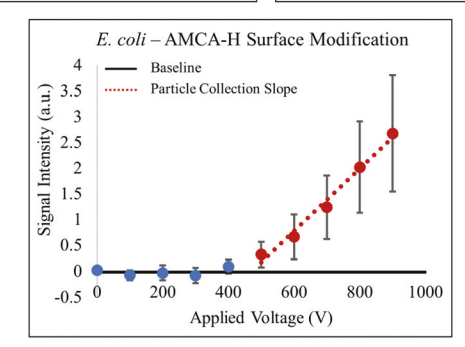
The velocity of the bacteria was determined using particle tracing in the open area of the device where there was no evidence of trapping, just prior to the gate of interest (Fig. 2). A linear fit was used with respect to the applied voltage to more

Paper Analyst









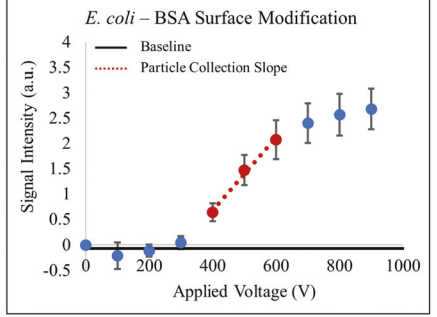


Fig. 3 The effect of varying the voltage on the trapping behavior of surface modified E. coli was assessed 10 seconds after the application of potential. A linear fit of trapping behavior was assessed (dotted red line) when the signal was significantly different than the baseline and prior to a plateau in signal intensity (see text for details). Data points represent the mean signal intensity of the region of interest for the individual trials and red data points indicate those which were used for the linear fit. The error bars represent the 95% CI. The absolute value of the applied potential is used for the plot.

Table 1 Biophysical properties of E. coli for each surface modification

Surface modification	$^{\mu_{\rm EK}}_{\left(\times10^{-8},{\rm m^2V^{-1}s^{-1}}\right)}$	Trapping onset voltage (V)	$(\times 10^{-17}, \mathrm{m}^4 \mathrm{V}^{-2} \mathrm{s}^{-1})$	$\frac{\mu_{\rm EK}}{\mu_{ m DEP}} \ (imes 10^9, { m V m^{-2}})$
None	3.0 ± 0.09	240 ± 66	1.2 ± 0.34	2.4 ± 0.66
Glycine	3.2 ± 0.07	270 ± 38	1.2 ± 0.17	2.7 ± 0.38
BSA	3.4 ± 0.1	310 ± 34	1.1 ± 0.12	3.1 ± 0.34
AMCA-H	5.1 ± 0.1	470 ± 46	1.1 ± 1.1	4.7 ± 0.46
Spermine	2.7 ± 0.09	460 ± 62	0.58 ± 0.081	$\textbf{4.6} \pm \textbf{0.62}$

accurately determine μ_{EK} and confirm consistent behavior over a range of velocities (Table 1). The μ_{EK} values ranged from 2.7 to $5.1 \times 10^{-8} \text{ m}^2 \text{ V}^{-1} \text{ s}^{-1}$ with approximately 3% relative standard deviation and were significantly different from each other (Table 1). All values of $\mu_{\rm EK}$ were close to $3.0 \times 10^{-8} \; {\rm m}^2 \; {\rm V}^{-1} \; {\rm s}^{-1}$, except for those modified with AMCA-H.

iDEP trapping experiments

Additional electrophysical behaviors of the surface modified E. coli were quantified in the iDEP microdevice. Data were collected while varying both the magnitude and the duration of the applied potential. In all cases the general structure of the trapping was consistent with previous comparable work, in that a characteristic crescent shape of collected bacteria was observed a few microns prior to the first 27 µm gate on the inlet side (Fig. 2C). No observable trapping behavior was observed at the 90 µm or larger gates for any experiments.

Trapping DEP is a result of a ratio of channel effects balancing or exceeding the intrinsic biophysical property ratio of the analyte (eqn (6)). The specific onset potential (c) that meets the trapping ratio results in the collection, or trapping, of the bacteria rather than its continued movement in the microchannel (eqn (6)). To evaluate the threshold, the I_s in a defined ROI surrounding the typical point of trapping was assessed after 10 s of applied voltage from -100 to -900 V in increments of 100 V. The baseline (no cells trapped) of I_s was determined using the following voltages: 0 to -200 V for no modification and glycine, 0 to -300 V for BSA, and 0 to -400 V for AMCA-H and spermine. The range of voltages for baseline determination varied as a function of the onset potential for each analyte. Trapping was defined as the point when the measured I_s was significantly greater than the baseline (2-tailed t-test, 95% confidence interval). The I_s initially increases linearly with applied potential at values higher than c (Fig. 3) and then plateaus except for the data from spermine and AMCA-H. All data sets

resulted in a consistent baseline prior to the onset of trapping and then a linear increase in the I_s with increased applied potential, which is consistent with what has been seen for other analytes previously studied in the field. 2,23,28,30,60-62 Furthermore, for each surface modification a sufficient linear range of trapped material was determined, which was statistically fit to determine c and the estimated error (Table 1). Combining the value of c and COMSOL models of the microchannels, the ratio of mobilities for each of the surface modifications are determined (Table 1). Utilizing the measured $\mu_{\rm EK}$ and ratio of mobilities, $\mu_{\rm DEP}$ is determined for each cell population (Table 1).

Data model and structure

Two independent determinations of μ_{EK} were performed. One was based on particle tracing measurements in the more open portions of the channel, where only electrokinetic effects are present, to determine \vec{v}_{EK} , and the other used the time-dependent data model (eqn (7)) to assess iDEP trapping data for each surface modification. The time-dependent data were limited to voltages where the I_s was statistically different than the baseline (red data points and linear fit, Fig. 3) and prior to the 'plateauing' (nonlinearities) in the data points, which occur at higher voltages (no modification, glycine, and BSA modifications). The higher voltage non-linear data were not included because collected material may have surpassed the limit of detection for the CCD of the ROI, material may have started to collect at the 60 µm gates, or particle-particle interactions may have interrupted trapping.

To calculate μ_{EK} using the time-dependent data model the following values were used: t as 10 s after the application of potential, h as 17 μ m, and \bar{E}_{ave} was determined using the applied potential and characteristic length of the microchannel. Given the approximate size of E. coli and the channel height, s can range from 1 to 34 cells, and is treated as an adjustable parameter given that the exact number of particles stacked when trapping occurs is dependent on the size and interactions of the bacteria. Alterations to s were made to align the values of μ_{EK} determined using the time-dependent model with those determined by velocity measurements. Assuming w of 0.2 mm, the $\mu_{\rm EK}$, within the 95% CI of the $\mu_{\rm EK}$ determined from the velocity measurements and s values (in parentheses), for the unmodified, glycine, and BSA modified bacteria were determined to be $3.0 \pm 0.9 \times 10^{-8}$, 14 $3.3 \pm 0.6 \times 10^{-8}$, 18 and $3.5 \pm 0.5 \times 10^{-8 \text{ } 16} \text{ m}^2 \text{ V}^{-1} \text{ s}^{-1}$, respectively. For the *E. coli* modified with spermine μ_{EK} was determined using a decreased w of 0.15 mm (see Experimental section) and s of 24, to be 2.6 \pm 0.7 \times 10^{-8} m² V⁻¹ s⁻¹ which is within the 95% CI of the $\mu_{\rm EK}$ determined using velocity. A comparable value for the μ_{EK} determined using the data model for the AMCA-H surface modified bacteria could not be determined within the bounds set for w and s.

Discussion

Modifying the surface of E. coli causes measurable differences in its biophysical properties. Utilizing iDEP both the μ_{EK} and $\mu_{\rm DEP}$ of the modified bacteria can be assessed to understand the changes to the biophysical properties (Fig. 3-5 and Table 1).

While a large variety of modifiers are available for cell surface modification using the carbodiimide reaction presented in this manuscript, the selection of each modifier was

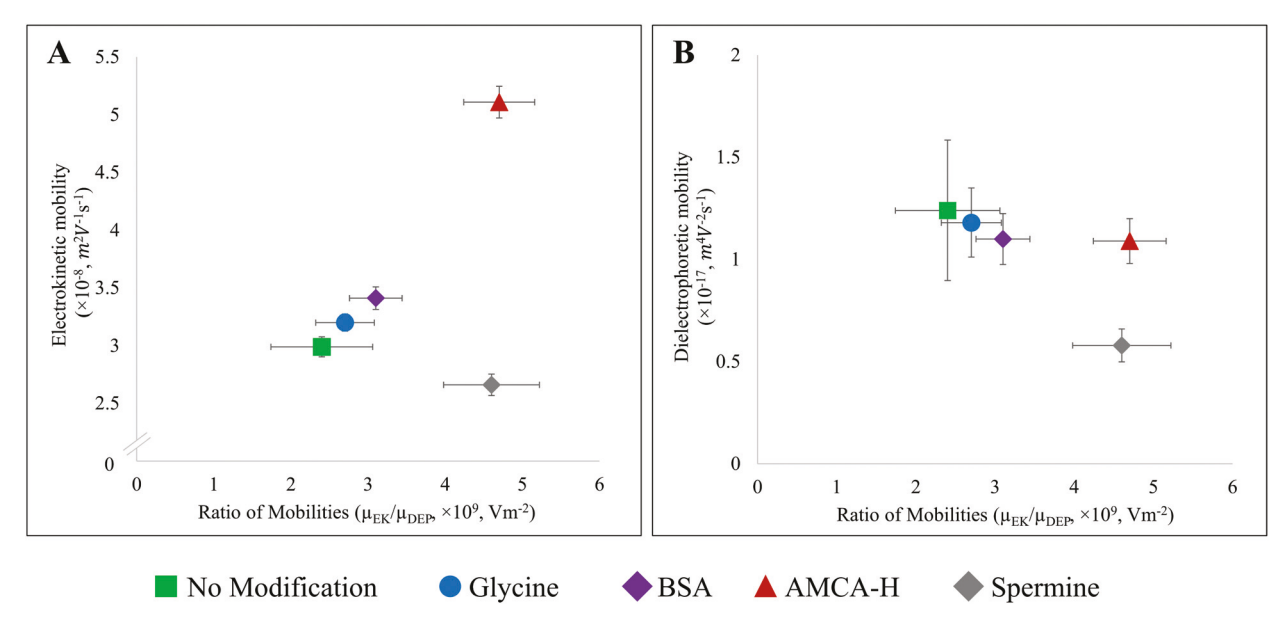


Fig. 4 Comparison of the electrokinetic (A) and dielectrophoretic (B) mobilities versus their trapping ratio for each surface label (note vertical axes). Each surface modification results in notably different electrokinetic mobilities, while only the AMCA-H and spermine's dielectrophoretic mobilities are different.

Paper

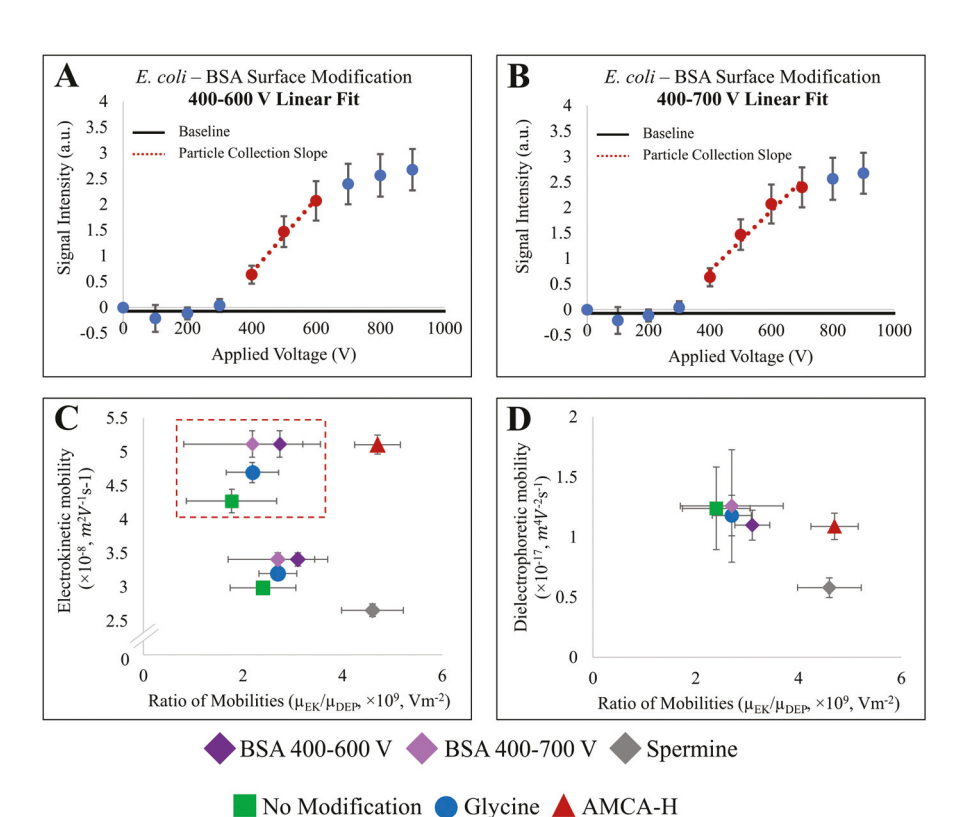


Fig. 5 iDEP trapping results for BSA modified *E. coli*. (A & B) The effect of various applied potentials at the first 27 μ m gate where t_A is 10 s, where the error bars represent the 95% CI. The absolute value of the applied potential is used for the plot. A linear fit either including or excluding V_A of -700 V can be assessed (see text for rationale). (C & D) Graphs depicting the trapping ratio *versus* the electrokinetic and dielectrophoretic mobilities (note vertical axes). The inset in the electrokinetic mobility graph (bottom left) depicts the error bars for the relevant surface modifications.

done to probe the system for its response to various attributes. Glycine was selected as it makes a minimal change to the surface chemistry, while maintaining the carboxyl surface group. Spermine was utilized to test for the ability to detect the effect of adding a hydrophobic sidechain which affects the cell's buffer capacity. BSA was selected for its size and to see the effects of adding a protein.

The $\bar{\nu}_{\rm EK}$ for each surface modification was determined, and by extension the $\mu_{\rm EK}$ (Table 1). Under these experimental conditions where all other influencing factors are held constant (buffer, device), the relative values of $\mu_{\rm EK}$ are a direct metric of the average charge density on the cell surface (eqn (1)). For each surface modification a statistically unique $\mu_{\rm EK}$ was determined, consistent with the unique modification for each reactant to the surface of the bacteria influencing or altering the cell (Fig. 4A). The $\mu_{\rm EK}$ for the AMCA-H modified *E. coli* is set apart from any other surface treatment which is expected because the AMCA-H treatment alters the viability of the cells (ESI†). Previously, the ability to differentiate between living and dead *E. coli* was attributed to changes in the conductivity of the cell membranes. 26

To further understand how surface modifications can affect the biophysical properties of *E. coli*, the trapping behavior of the bacteria in an iDEP microchannel was assessed (Fig. 3). In comparison to the $\mu_{\rm EK}$, the $\mu_{\rm DEP}$ is statistically unaffected when comparing the unmodified bacteria with those modified with

the glycine, BSA, or AMCA-H; while those modified with spermine result in a statistically significant change in μ_{DEP} (Fig. 4B).

The $\mu_{\rm DEP}$ can be affected by both the external and internal properties of the cell. Specifically, when under DC conditions, changes to the conductivity of the cell will influence the μ_{DEP} . In the case of biological analytes the effect of conductivity is generally assessed using the multi-shell model to account for the effect of the cytoplasm, membrane, and cell wall. 17,48,49 The conductivity relate to the ability of a given particle to conduct electricity and store electrical energy, respectively. This suggests that as spermine results in a statistically significant shift in μ_{DEP} , it is possible that this modification resulted in changes to both the external and internal properties of the bacteria. Additionally, the spermine modification adds a long hydrophobic chain to the surface of the cell, while all of the other modifications tested in this manuscript were hydrophilic. The addition of spermine also alters the buffering capacity of the cell, as the cell no longer has the carboxyl group necessary for buffering at low pH's, but is able to buffer at higher pH's.57 It should be noted that previous work correlated the difference in cell behavior to only the conductivity of the cell membrane, which would be an external cell property. 63 Furthermore, it is interesting that for all the modified cells there is a decrease in the measured μ_{DEP} in comparison to the unmodified cells.

It should be noted that for assessments using iDEP there is an advantage to using simple microchannels with fewer constrictions. This can help to decrease the voltage necessary to achieve the necessary trapping condition represented by eqn (6) and reduce undesirable non-linear effects.⁶⁴ However, for the purposes of this manuscript a general use device was implemented to determine the ability of iDEP to help understand the effect of surface modifications on biophysical properties. Developing a microdevice with fewer constrictions to probe other surface modifications in the future would be advantageous but was not necessary for this assessment.

The slope of the time-dependent data is proportional to μ_{EK} (Fig. 3 and eqn (7)). As s is a bracketed (reasonable values are only from 1 to 34) adjustable parameter, it can be used to validate the data. For the cases of the unmodified E. coli and those modified with glycine or BSA the value of s ranged from 22-26 to generate results which were within the 95% CI of the velocity-based measurements.

This method of determining μ_{EK} can also give insight to the experimental data. For instance, with the spermine modified E. coli no reasonable values (between 1 and 34) of s with a w of 0.2 mm matched with the velocity-based values. This is because the spermine modified E. coli have a smaller velocity than the other modifications and therefore, due to the gradient gate design of the channel, will experience a smaller w (eqn (7)). Reducing w to 0.15 mm allowed an s value of 24 to be within the statistical 95% CI of the velocity-based value.

For the AMCA-H modified E. coli, no reasonable value for $\mu_{\rm EK}$ could be determined using the data model with the set constraints on w and s. Potential factors which may be affecting this include the fact that the average \vec{v}_{EK} and thus μ_{EK} was significantly higher than for any other treatment (Table 1). Furthermore, the AMCA-H modified cells were prone to aggregation during trapping, which resulted in the aggregates leaving the initial gate of trapping, affecting the assessed I_s . Furthermore, as the AMCA-H modified cells were no longer viable, the integrity of the cell structure may have been compromised, which could affect the applicability of the model.

The adjustable parameter s is similar to correction factors which have been used by other groups when determining the trapping condition. 65-67 Correction factors have been found to depend on the size, shape, and deformability of the analyte of interest. In various models, the need for a correction factor generally arises from either an underestimation of the dielectrophoretic velocity, or an overestimation of the electrokinetic velocity. 66 The model used in this paper appears to be overestimating the $\bar{\nu}_{EK}$, which can be seen for glycine and BSA modified bacteria. This however is not seen for the spermine modified bacteria. This may be due to the change in w, which might have therefore resulted in an underestimation of the dielectrophoretic velocity. The correction factors utilized in this paper are similar to those found by other groups previously. 65,66 The $\bar{\nu}_{\text{EK}}$ determined using the model presented in this paper did result in values that fell within the statistical 95% CI of the velocity-based value, suggesting that this model

can fairly accurately determine $\vec{\nu}_{EK}$, and therefore assess the effect of the surface modifications to the bacteria.

Data consideration and interpretation

When working with micro- and nano-liters of sample maintaining a perfectly consistent environment is impossible regardless of the expertise of a researcher. Challenges with evaporation (especially with high potentials applied), balancing of flow, and consistent device creation will all affect the collected data. For example, when determining the μ_{EK} , using either velocity measurements or the data model, the effect of residual pressure driven flow must be considered. Care was taken during experimentation to minimize this effect, however a perfect balance is not always possible. In the case that pressure driven flow could not be completely eliminated, flow towards the outlet (forward flow) rather than inlet (backward flow) was preferred to prevent the reassessment of any previously trapped bacteria. In the case of velocity measurements, forward pressure driven flow would artificially increase the assessed $\vec{v}_{\rm EK}$ and thus $\mu_{\rm EK}$. In the case of the data model, pressure driven flow would add to the electrokinetic effects in the channel resulting in a higher onset potential and therefore a larger ratio of mobilities. Furthermore, the presence of forward pressure driven flow would increase the rate of trapping, artificially making the slope of the trapped data steeper (Fig. 3). All of these facts will affect the accuracy of the assessment of μ_{EK} using either velocity estimation or the data model.

As with most scientific techniques for analysis, including iDEP, the interpretation of data is key to understanding the results of any given experiment. Given that iDEP is a fairly young field, a set method for data interpretation has not been widely accepted in the field. Therefore, we will discuss challenges in using the method of interpretation utilized in this paper.

For the data presented herein, the assessment of the linear region (Fig. 3) requires an iterative process to select an appropriate fit of the statistically significant trapping. The linear fit ultimately incorporates the maximum amount of data where statistical trapping is occurring, while maintaining a realistic fit. In some cases an obvious plateau in data is observed, which is the case for unmodified and glycine modified E. coli (Fig. 3). However, for the BSA modified E. coli the start of the plateau is semi-ambiguous. It should be noted that for the bacteria modified with BSA a total of 20 replicate trials were performed, whereas for all other surface modifications 9-13 replicates were obtained. The data for -700 V can potentially be incorporated into the linear fit or deemed as part of the data plateau (Fig. 5A & B).

Several factors come into play when determining the best fit. The coefficient of determination for the individual trials is slightly better for -400 to -600 V fit ($R^2 = 0.58$ vs. 0.52). Furthermore, c was determined for both fits, and their 95% CI, resulting in -310 ± 34 V and -270 ± 100 V for the -400 to -600 V and the -400 to -700 V fits, respectively. Based on the slightly better fit and the smaller range for c the -400 to -600

Paper Analyst

V assessment is primarily discussed in this paper. The smaller range of c is a logical choice as more replicates should decrease the range depicted by the 95% CI. In this case the -400 to -600 V interpretation has a 95% CI interval similar to the other surface modifications, while the -400 to -700 V fit results in the largest range.

Altering the linear fit will affect c and therefore the ratio of mobilities and μ_{DEP} (Fig. 5C & D). When looking at the μ_{EK} and ratio of mobilities (Fig. 5C) the understanding of results does not significantly shift as each modification occupies its own unique space relative to the other modifications. Similarly, for the comparison of μ_{DEP} and the ratio of mobilities (Fig. 5D) spermine is still the only modification which is significantly altered. A significant shift in μ_{DEP} for BSA modified *E. coli* is not observed. For comparison $\mu_{\rm DEP}$ is 1.1 \pm 0.12 \times 10⁻¹⁷ and $1.3 \pm 0.47 \times 10^{-17} \text{ m}^4 \text{ V}^{-2} \text{ s}^{-1}$ for the -400 to -600 V and the -400 to -700 V assessments, respectively. For the BSA modified E. coli the choice of linear fit does not greatly change the results. To potentially improve upon the accuracy of the assessed values of c and $\mu_{\rm DEP}$, $I_{\rm s}$ could be assessed every 50 V.

Conclusion

This work utilizes iDEP to determine the biophysical effects of surface modifications to E. coli. Shifts in μ_{EK} are generally associated with the external properties of the cell which is confirmed in this work. Whereas, μ_{DEP} is influenced by both internal and external properties of the analyte. A reasonable expectation for each of these surface modifications would be that μ_{EK} changes but the μ_{DEP} may or may not be changed. Results consistent with this expectation were observed here. Independent determination of the zeta potential and conductivity will allow more detailed interpretation of the changes induced in the cells. Furthermore, the loading efficiency of the various modifications onto the cell should be probed to determine the limit of detection possible with iDEP. It is important to note that these subtle changes in the cell properties were differentiated with an un-labeled, un-biased, and non-destructive method to determine the biophysical properties of the cells.

Abbreviations

DEP Dielectrophoresis

iDEP Insulator-based dielectrophoresis

EP Electrophoresis EO Electroosmosis EK Electrokinetic

Electrokinetic mobility $\mu_{\rm EK}$ Electrophoretic mobility $\mu_{\rm EP}$ Electroosmotic mobility $\mu_{\rm EO}$ Dielectrophoretic mobility μ_{DEP} $F_{
m DEP}$ Dielectrophoretic force Clausius-Mossotti factor $f_{\rm CM}$ $\bar{\nu}_{\rm EK}$ Electrokinetic velocity

 $\vec{\nu}_{\mathrm{DEP}}$ Dielectrophoretic velocity \vec{E} Electric field strength

 $\nabla \left| \vec{\bar{E}} \right|^2$ Gradient of the electric field squared

E. coli Escherichia coli

Conflicts of interest

C. V. C. and M. A. H. declare an interest in Charlot Biosciences, a company which is seeking to commercialize the design and function of the microfluidic chips used in this paper.

Acknowledgements

The authors acknowledge the facilities and staff at the Center for Solid State Electronic Research (CSSER) for assistance with microfluidic fabrication. This work was supported by NSF grant 1644328 and NIH grants R03AI111361-01 and 1R21AI130855-01A1.

References

- 1 J. Ding, C. Woolley and M. A. Hayes, Anal. Bioanal. Chem., 2017, 409, 6405-6414.
- 2 P. V. Jones, S. H. Hilton, P. E. Davis, R. Yanashima, R. McLemore, A. McLaren and M. A. Hayes, Analyst, 2015, 140, 5152-5161.
- 3 X. Hu, P. H. Bessette, J. Qian, C. D. Meinhart, P. S. Daugherty and H. T. Soh, Proc. Natl. Acad. Sci. U. S. A., 2005, 102, 15757.
- 4 J. Johari, Y. Hübner, J. C. Hull, J. W. Dale and M. P. Hughes, Phys. Med. Biol., 2003, 48, N193.
- 5 A. A. S. Bhagat, H. Bow, H. W. Hou, S. J. Tan, J. Han and C. T. Lim, Med. Biol. Eng. Comput., 2010, 48, 999-1014.
- 6 J. Bauer, J. Chromatogr. B: Biomed. Sci. Appl., 1987, 418, 359-383.
- 7 Z. R. Gagnon, Electrophoresis, 2011, 32, 2466-2487.
- 8 K. H. Lee, K. S. Lee, J. H. Jung, C. B. Chang and H. J. Sung, Appl. Phys. Lett., 2013, 102, 141911.
- 9 M. J. Tomlinson, S. Tomlinson, X. B. Yang and J. Kirkham, J. Tissue Eng., 2012, 4, 2041731412472690.
- 10 M. G. Roper, Anal. Chem., 2016, 88, 381-394.
- 11 J. Sibbitts, K. A. Sellens, S. Jia, S. A. Klasner and C. T. Culbertson, Anal. Chem., 2018, 90, 65-85.
- 12 R. Pethig, Biomicrofluidics, 2010, 4, 022811.
- 13 J.-P. Hsu, T.-S. Hsieh, T.-H. Young and S. Tseng, Electrophoresis, 2003, 24, 1338-1346.
- 14 S.-I. Han, H. Soo Kim and A. Han, Biosens. Bioelectron., 2017, 97, 41-45.
- 15 X. Chen, Z. Liang, D. Li, Y. Xiong, P. Xiong, Y. Guan, S. Hou, Y. Hu, S. Chen, G. Liu and Y. Tian, Biosens. Bioelectron., 2018, 99, 416-423.
- 16 A. LaLonde, M. F. Romero-Creel and B. H. Lapizco-Encinas, Electrophoresis, 2015, 36, 1479-1484.

- 17 S. H. Hilton and M. A. Hayes, Anal. Bioanal. Chem., 2019, 411, 2223–2237.
- 18 E. B. Cummings and A. K. Singh, *Anal. Chem.*, 2003, 75, 4724–4731.
- 19 P. V. Jones and M. A. Hayes, *Electrophoresis*, 2015, 36, 1098–1106.
- 20 A. LaLonde, A. Gencoglu, M. F. Romero-Creel, K. S. Koppula and B. H. Lapizco-Encinas, *J. Chromatogr., A*, 2014, **1344**, 99–108.
- 21 S. K. Srivastava, J. L. Baylon-Cardiel, B. H. Lapizco-Encinas and A. R. Minerick, *J. Chromatogr.*, A, 2011, 1218, 1780–1789.
- 22 M. Kim, T. Jung, Y. Kim, C. Lee, K. Woo, J. H. Seol and S. Yang, *Biosens. Bioelectron.*, 2015, 74, 1011–1015.
- 23 A. LaLonde, M. F. Romero-Creel, M. A. Saucedo-Espinosa and B. H. Lapizco-Encinas, *Biomicrofluidics*, 2015, **9**, 064113.
- 24 H. Li and R. Bashir, Sens. Actuators, B, 2002, 86, 215-221.
- 25 D. S. Gray, J. L. Tan, J. Voldman and C. S. Chen, *Biosens. Bioelectron.*, 2004, **19**, 1765–1774.
- 26 B. H. Lapizco-Encinas, B. A. Simmons, E. B. Cummings and Y. Fintschenko, *Anal. Chem.*, 2004, **76**, 1571–1579.
- 27 C.-F. Chou, J. O. Tegenfeldt, O. Bakajin, S. S. Chan, E. C. Cox, N. Darnton, T. Duke and R. H. Austin, *Biophys. J.*, 2002, 83, 2170–2179.
- 28 P. V. Jones, A. F. DeMichele, L. Kemp and M. A. Hayes, Anal. Bioanal. Chem., 2014, 406, 183–192.
- 29 B. H. Lapizco-Encinas, R. V. Davalos, B. A. Simmons, E. B. Cummings and Y. Fintschenko, *J. Microbiol. Methods*, 2005, **62**, 317–326.
- 30 W. A. Braff, D. Willner, P. Hugenholtz, K. Rabaey and C. R. Buie, *PLoS One*, 2013, 8, e76751.
- 31 J. N. Mehrishi and J. Bauer, *Electrophoresis*, 2002, **23**, 1984–1994.
- 32 C. Wagner and M. Hensel, in *Bacterial Adhesion: Chemistry*, *Biology and Physics*, ed. D. Linke and A. Goldman, Springer, Netherlands, Dordrecht, 2011, pp. 17–34.
- 33 N. Mozes, A. Léonard and P. G. Rouxhet, *Biochim. Biophys. Acta, Biomembr.*, 1988, **945**, 324–334.
- 34 X. B. Wang, Y. Huang, X. J. Wang, F. F. Becker and P. R. C. Gascoyne, *Biophys. J.*, 1997, 72, 1887–1899.
- 35 L. M. H. Prescott, J. P. Klein and D. A. Klein, *Microbiology*, Wm. C. Brown Publishers, Dubuque, IAA, 1996.
- 36 A. G. Moat, J. W. Foster and M. P. Spector, *Microbial Physiology*, Wiley-Liss, New, York, 4th edn, 2002.
- 37 J. Suehiro, R. Hamada, D. Noutomi, M. Shutou and M. Hara, *J. Electrost.*, 2003, 57, 157–168.
- 38 R. Sonohara, N. Muramatsu, H. Ohshima and T. Kondo, *Biophys. Chem.*, 1995, 55, 273–277.
- 39 B. Buszewski, M. Szumski, E. Kłodzińska and H. Dahm, *J. Sep. Sci.*, 2003, **26**, 1045–1049.
- 40 M. Torimura, S. Ito, K. Kano, T. Ikeda, Y. Esaka and T. Ueda, *J. Chromatogr. B: Biomed. Sci. Appl.*, 1999, 721, 31–37.
- 41 E. Kłodzińska, M. Szumski, E. Dziubakiewicz, K. Hrynkiewicz, E. Skwarek, W. Janusz and B. Buszewski, *Electrophoresis*, 2010, 31, 1590–1596.

- 42 C. V. Crowther and M. A. Hayes, *Analyst*, 2017, **142**, 1608-1618
- 43 H. A. Pohl and J. S. Crane, *Biophys. J.*, 1971, **11**, 711–727
- 44 H. A. Pohl, *Dielectrophoresis: the behavior of neutral matter in nonuniform electric fields*, Cambridge University Press, Cambridge, New York, 1978.
- 45 S. Srivastava, A. Gencoglu and A. Minerick, *Anal. Bioanal. Chem.*, 2011, **399**, 301–321.
- 46 T. B. Jones, *Electromechanics of Particles*, Cambridge University Press, 1995.
- 47 R. W. Clarke, J. D. Piper, L. Ying and D. Klenerman, *Phys. Rev. Lett.*, 2007, **98**, 198102.
- 48 A. Irimajiri, T. Hanai and A. Inouye, *J. Theor. Biol.*, 1979, 78, 251–269.
- 49 W. Bai, K. Zhao and K. Asami, *Colloids Surf.*, B, 2007, 58, 105–115.
- 50 H. Ji-Ping, Y. Kin-Wah, L. Jun and S. Hong, *Commun. Theor. Phys.*, 2002, 38, 113.
- 51 J. P. Huang, K. W. Yu, G. Q. Gu and M. Karttunen, *Phys. Rev. E: Stat.*, *Nonlinear, Soft Matter Phys.*, 2003, **67**, 051405.
- 52 C. V. Crowther, S. H. Hilton, L. Kemp and M. A. Hayes, *Anal. Chim. Acta*, 2019, **1068**, 41–51.
- 53 M. D. Pysher and M. A. Hayes, *Anal. Chem.*, 2007, **79**, 4552–4557.
- 54 S. J. R. Staton, K. P. Chen, J. P. Taylor, J. R. Pacheco and M. A. Hayes, *Electrophoresis*, 2010, 31, 3634–3641.
- 55 S. J. R. Staton, P. V. Jones, G. Ku, D. S. Gilman, I. Kheterpal and M. A. Hayes, *Analyst*, 2012, **137**, 3227–3229.
- 56 L. Siegmund and J. Wöstemeyer, *Understanding bacterial uptake by protozoa: A versatile technique for surface modification of bacteria*, 2016.
- 57 L. Siegmund, M. Schweikert, M. S. Fischer and J. Wöstemeyer, *J. Eukaryotic Microbiol.*, 2018, **66**, 600–611.
- 58 K. A. Majorek, P. J. Porebski, A. Dayal, M. D. Zimmerman, K. Jablonska, A. J. Stewart, M. Chruszcz and W. Minor, *Mol. Immunol.*, 2012, 52, 174–182.
- 59 J.-D. Pédelacq, S. Cabantous, T. Tran, T. C. Terwilliger and G. S. Waldo, *Nat. Biotechnol.*, 2005, 24, 79.
- 60 J. Ding, R. M. Lawrence, P. V. Jones, B. G. Hogue and M. A. Hayes, *Analyst*, 2016, 141, 1997–2008.
- 61 P. V. Jones, S. J. R. Staton and M. A. Hayes, *Anal. Bioanal. Chem.*, 2011, **401**, 2103–2111.
- 62 C. V. Crowther, S. H. Hilton, L. Kemp and M. A. Hayes, *Anal. Chim. Acta*, 2019, **1068**, 41–51.
- 63 B. H. Lapizco-Encinas, B. A. Simmons, E. B. Cummings and Y. Fintschenko, *Electrophoresis*, 2004, 25, 1695–1704.
- 64 V. H. Perez-Gonzalez, R. C. Gallo-Villanueva, B. Cardenas-Benitez, S. O. Martinez-Chapa and B. H. Lapizco-Encinas, *Anal. Chem.*, 2018, **90**, 4310–4315.
- 65 M. A. Saucedo-Espinosa and B. H. Lapizco-Encinas, *Electrophoresis*, 2015, **36**, 1086–1097.
- 66 N. Hill and B. H. Lapizco-Encinas, *Electrophoresis*, 2019, **40**, 2541–2552.
- 67 M. Mohammadi, H. Madadi, J. Casals-Terré and J. Sellarès, *Anal. Bioanal. Chem.*, 2015, **407**, 4733–4744.